CHEMISTRY
AN ASIAN JOURNAL
ACES
FULL PAPER

DOI: 10.1002/asia.201300328

New Dual Donor–Acceptor (2D-π-2A) Porphyrin Sensitizers for Stable and Cost-Effective Dye-Sensitized Solar Cells

Ram B. Ambre,[a] Gao-Fong Chang,[a] Manoj R. Zanwar,[b] Ching-Fa Yao,[b] Eric Wei-Guang Diau,*[c] and Chen-Hsiung Hung*[a]

Abstract: A series of porphyrin sensitizers that featured two electron-donating groups and dual anchoring groups that were connected through a porphine π-bridging unit have been synthesized and successfully applied in dye-sensitized solar cells (DSSCs). The presence of electron-donating groups had a significant influence on their spectroscopic, electrochemical, and photovoltaic properties. Overall, the dual anchoring groups gave tunable electronic properties and stronger attachment to TiO_2. These new dyes were readily synthesized in a minimum number of steps in gram-scale quantities. Optical and electrochemical data confirmed the advantages of these dyes for use as sensitizers in DSSCs. Porphyrins with electron-donating amino moieties provided improved charge separation and better charge-injection efficiencies for the studied dual-push–pull dyes. Attenuated total reflectance–Fourier-transform infrared (ATR-FTIR) and X-ray photoelectron spectroscopy of the porphyrin dyes on TiO_2 suggest that both *p*-carboxyphenyl groups are attached onto TiO_2, thereby resulting in strong attachment. Among these dyes, *cis*-Zn2BC2A, with two electron-donating 3,6-ditertbutyl-phenyl-carbazole groups and dual-anchoring *p*-carboxyphenyl groups, showed the highest efficiency of 4.07%, with $J_{SC=}9.81\,mA\,cm^{-2}$, $V_{OC}=0.63\,V$, and $FF=66\%$. Our results also indicated a better photostability of the studied dual-anchored sensitizers compared to their mono-anchored analogues under identical conditions. These results provide insight into the developments of a new generation of high-efficiency and thermally stable porphyrin sensitizers.

Keywords: donor–acceptor systems · dyes/pigments · porphyrins · sensitizers · solar cells

Introduction

In 1991, O′Regan and Grätzel introduced DSSCs as a potential competitor to the conventional silicon solar cell.[1] The design and synthesis of highly efficient sensitizers for DSSCs is one of the most attractive and challenging fields of research. Thousands of ruthenium, porphyrins, and organic dyes have been synthesized and utilized for dye-sensitized solar cells.[2] Devices that use ruthenium sensitizers N3,[3] N719,[3] C101,[4] C102,[4] C106,[5] and black dye[6] have achieved the highest efficiencies of about 11%, but their practical application is substantially hindered because of limited resources and the high cost of ruthenium metal. Organic dyes have attracted much attention in recent years because of their ease of synthesis, high molar extinction coefficients, and lower synthetic cost.[2d,f] However, the performance of organic dyes remains inferior to ruthenium and porphyrin metal complexes in terms of efficiency and stability. Indoline-containing D205[7] and triphenylamine (TPA)-containing C219[8] have given the highest efficiencies of 9.5% and 10.3%, respectively.

The unique properties of porphyrins, including strong Soret and moderate Q bands, fast electron injection, and good photophysical and thermal stability, make them ideal candidates for photovoltaic applications.[2b] Moreover, porphyrins are highly versatile molecules, the physicochemical properties of which can be tuned by the selective functionalization and chemical modification of their four *meso* and eight β-pyrrolic positions. An impressive efficiency of 7.8% was achieved by β-pyrrolic-malonic-acid-substituted zinc porphyrins.[9] Recently, porphyrins with a push–pull system (D-π-A) have become popular because of their ease of modulation on electron-donating and anchoring sites, through which their optical, electrochemical, and photochemical properties can be tuned to afford high efficiencies.[10] By utilizing a similar concept, Bessho et al. reported porphyrin sensitizer YD2, which gave a power-conversion efficiency of 11%.[10e] The record-breaking efficiency of 12.3% was achieved by mixing YD2-*o*-C8 porphyrin sensi-

[a] R. B. Ambre, G.-F. Chang, Dr. C.-H. Hung
Institute of Chemistry, Academia Sinica
Nankang Taipei, 115 (Taiwan)
Fax: (+886) 2-27831237
E-mail: chhung@gate.sinica.edu.tw

[b] M. R. Zanwar, Prof. C.-F. Yao
Department of Chemistry, National Taiwan Normal University
Taipei, 11677 (Taiwan)

[c] Prof. E. W.-G. Diau
Department of Applied Chemistry and
Institute of Molecular Science
National Chiao Tung University
Hsinchu, 300 (Taiwan)
E-mail: diau@mail.nctu.edu.tw

Supporting information for this article is available on the WWW under http://dx.doi.org/10.1002/asia.201300328.

tizer with an organic dye in a cobalt-based electrolyte.[11] However, the syntheses of YD2 and YD2-*o*-C8 require several steps, including key reactions of Sonogashira and Buchwald–Hartwig cross-coupling reactions, which might make the mass production of these porphyrin dyes infeasible. Moreover, the long-term thermal stability of YD2 and YD2-*o*-C8 is a concern, owing to their ethynyl bridging group and single *p*-carboxyphenyl unit for attachment onto TiO_2. Therefore, it is our objective to design sensitizers in a minimum number of steps in high yields and with good thermal stabilities for mass production and long-term use.

As a part of our ongoing project on the development of cost-effective, highly efficient, and stable sensitizers for DSSCs, our previously studied sensitizers 3S1A, *trans*-2S2A, *cis*-2S2A, and 1S3A, revealed dominating effects of electron mediation and the binding mode of *p*-carboxyphenyl groups, which strongly controlled the overall efficiencies of the DSSCs.[12] Among these four derivatives, *cis*-2S2A and 1S3A, which possessed two or more *p*-carboxyphenyl groups at their *meso* positions, showed the highest conversion efficiencies of 2.5% and 3.0%, respectively. Our results demonstrated that the performance of these DSSCs could be effectively enhanced by the incorporation of more than one anchoring sites onto the sensitizing dyes through a superior electron-injection efficiency and higher voltage compared to single-arm-attached 3S1A and *trans*-2S2A. This finding is consistent with the structures of highly efficient ruthenium sensitizers N3, N719, and C106, all of which contain two or more carboxy anchoring groups.[3,5] Notably, even though they contain a single anchoring arm, exceptional efficiencies can be achieved on porphyrin sensitizers YD2 and YD2-*o*-C8 with a D-π-A framework, in which the electron-rich moiety is attached onto the donating side of porphyrin, whereas the electron-deficient moiety is attached onto the anchoring side.[10e,11] During the operation of the DSSC, upon illumination, the excited electron from the sensitizer is transferred from the electron-donating groups to the acceptor units and is injected into the conduction band of TiO_2. However, in most of the reported push–pull dyes, only one anchoring group is present with respect to multiple electron-donating *meso* substituents, which could lead to non-tunable interfacial electron transfer.[13] Furthermore, dye desorption has been observed in single-armed D-π-A systems, which may be a significant drawback for their future commercialization. Herein, we aimed to combine dual anchoring groups with the push–pull D-π-A framework to deliver a new class of 2D-π-2A porphyrin sensitizers that contained two electron-donating moieties and two anchoring moieties connected by a porphine core as the π bridge, namely, *cis*-Zn2T2A, *cis*-Zn2U2A, *cis*-Zn2TH2A, *cis*-Zn2TC2A, *cis*-Zn2BC2A, and *cis*-Zn2TPA2A (Scheme 1).

Results and discussions

Syntheses of 2D-π-2A Porphyrin Sensitizers

The synthetic routes to the studied 2D-π-2A porphyrins are shown in Scheme 2. Porphyrin sensitizers *cis*-Zn2T2A, *cis*-Zn2U2A, *cis*-Zn2TH2A, *cis*-Zn2TC2A, *cis*-Zn2BC2A, and *cis*-Zn2TPA2A were synthesized in three steps: mixed condensation,[14] zinc metalation,[15] and hydrolysis.[16] The condensation reaction between pyrrole, methyl 4-formylbenzoate, and a corresponding aldehyde under Lindsey's conditions, catalyzed by boron trifluoride diethyl etherate, followed by subsequent oxidation with 2,3-dichloro-5,6-dicyano-1,4-benzoquinone (DDQ) afforded a mixture of six porphyrins. All of these porphyrins were characterized by optical, ATR-FTIR, and NMR spectroscopy and by HRMS. In the ATR-FTIR spectra, the obtained *cis*-porphyrins with ester derivatives (*cis*-2X2E) showed a stretching frequency at around 1720 cm^{-1}, thus supporting the presence of ester carbonyl groups. In the UV/Vis spectra, these free-base porphyrins showed a single strong Soret band and four moderate Q bands. Comprehensive characterization of all of the

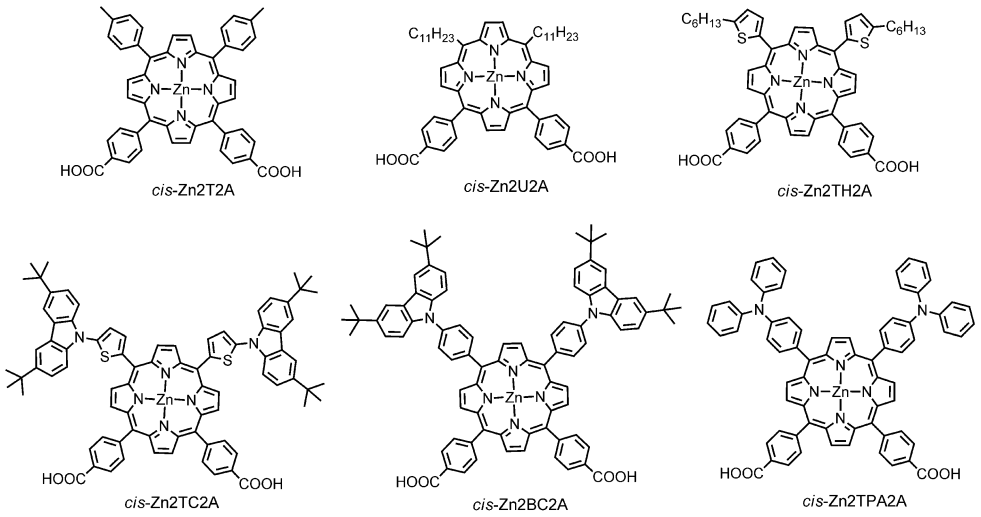

Scheme 1. Molecular structures of the dual donor–acceptor 2D-π-2A porphyrin dyes.

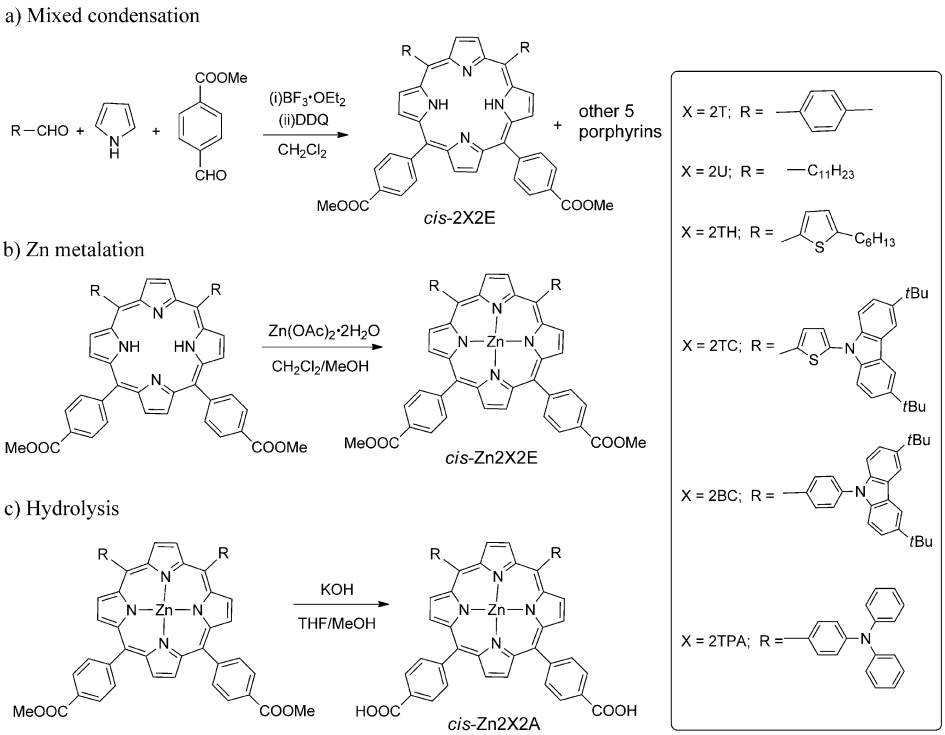

Scheme 2. Synthetic route to the studied 2D-π-2A porphyrin sensitizers.

products is provided in the Supporting Information. The subsequent zinc-metalation step to yield the zinc-metalated *cis*-ester derivatives of the porphyrins (*cis*-Zn2X2E) has been readily achieved in high yields by reacting a free-base porphyrin with zinc acetate. The success of zinc metalation of all the porphyrins was confirmed by UV/Vis and NMR spectroscopy and HRMS. UV/Vis spectra of the *cis*-Zn2X2E porphyrin products only showed one Soret band and two Q bands, whereas, in the NMR spectra, the inner NH resonance disappeared completely with slight upfield shifts of all of the remaining protons. Hydrolysis of the metal complexes to afford the *cis* dual-acid zinc porphyrins (*cis*-Zn2X2A) as the final products was easily achieved by reacting metal complexes in a mixture of THF and MeOH with excess aqueous KOH. The final products were confirmed by the disappearance of the methyl protons of the ester in NMR spectra and by HRMS. ATR-FTIR spectra of the final acid products showed shifting of the carbonyl peaks to 1675–1700 cm^{-1}, owing to intermolecular hydrogen bonding.

Optical Spectroscopy

The UV/Vis spectra of these porphyrins show a single intense Soret band and two moderate Q bands (Figure 1 a). The peak positions and their molar absorption coefficients (ε) are listed in Table 1. The shifts in the absorption bands of the porphyrins are substituent-dependent. The Soret bands are slightly red-shifted and broadened for porphyrins with stronger electron-donating groups. The molar absorption coefficient of *cis*-Zn2BC2A is the highest among all of the porphyrins considered, which has a significant influence on its overall conversion efficiency (see below). The steady-state fluorescence spectra of all of the porphyrins in THF, upon excitation at the Soret band, displayed a similar trend to the UV/Vis spectra, with a red-shift for electron-donating-group-substituted complexes. Notably, the dramatic red-shift of the fluorescence spectrum of *cis*-Zn2TC2A in comparison with that of *cis*-Zn2BC2A suggests that the thiophene group can act as a more efficient linker for mediating the electron communication with the porphyrin-conjugated system than the phenyl substituent.

The absorption spectra of these porphyrins as thin films

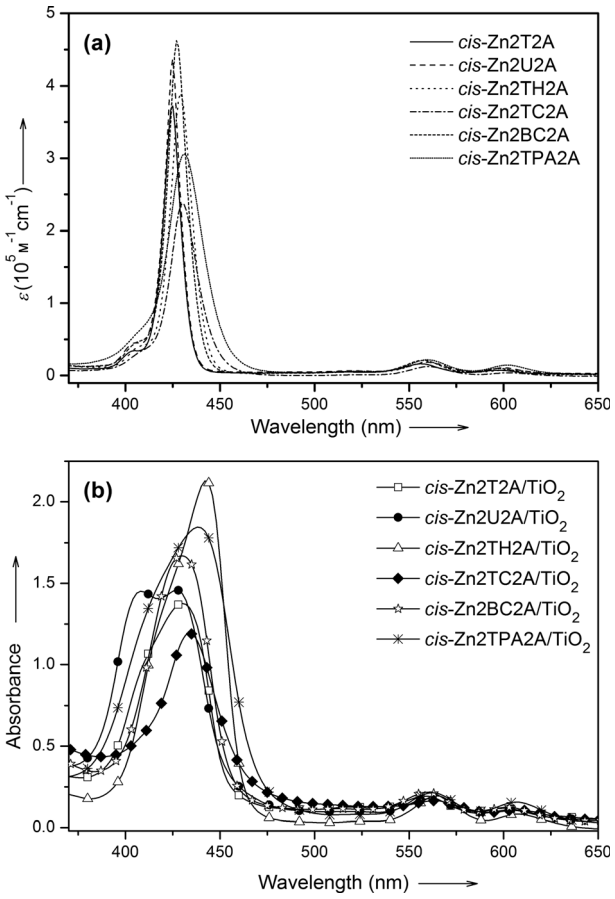

Figure 1. a) UV/Vis spectra of the studied porphyrins in THF. b) UV/Vis spectra of the studied porphyrins on TiO_2.

Table 1. Optical and electrochemical properties of 2D-π-2A porphyrins.

Dye	λ_{abs}[a] [nm] (ε [$\times 10^3$ M^{-1}cm^{-1}])	λ_{em}[b] [nm]	E_{ox}[c] [V]	$E_{0\text{-}0}$[d] [V]	E_{ox}*[e] [V]
cis-Zn2T2A	424 (368) 556 (16) 597 (7)	605 655	0.91	2.06	−1.14
cis-Zn2U2A	425 (436) 559 (18) 600 (11)	606 652	0.69	2.05	−1.36
cis-Zn2TH2A	429 (390) 560 (19) 601 (8)	618	0.90	2.03	−1.13
cis-Zn2TC2A	430 (238) 561 (12) 603 (4)	625 659	0.79	2.03	−1.24
cis-Zn2BC2A	427 (462) 557 (20) 599 (9)	607 658	0.93	2.06	−1.13
cis-Zn2TPA2A	430 (304) 560 (22) 602 (14)	616	0.70 0.88	2.04	−1.34

[a] Absorption maximum of the porphyrin in THF. [b] Emission maximum in THF by exciting at the Soret band. [c] First oxidation potentials, as determined by CV in THF (versus NHE). [d] $E_{0\text{-}0}$ values were estimated from the intersection of the absorption and emission spectra. [e] Excited-state oxidation potentials as approximated from the E_{ox} and $E_{0\text{-}0}$ values.

were studied to understand their adsorption behavior on TiO_2 (Figure 1b). The position and shape of the porphyrin peaks largely differ on TiO_2 thin films. Red-shifts of 2–13 nm in the Soret bands and 2–4 nm in the Q bands are observed with broadening of the peaks. Specifically, the spectra of *cis*-Zn2TPA2A/TiO_2 and *cis*-Zn2TH2A/TiO_2 are significantly broadened and red-shifted by 8 nm and 13 nm, respectively, compared to their spectra in THF, whereas the peaks of *cis*-Zn2T2A/TiO_2, *cis*-Zn2TC2A/TiO_2, and *cis*-Zn2BC2A/TiO_2 are also broadened and red-shifted by 2–6 nm. These patterns suggest a J-type aggregation with side-by-side porphyrin arrangements when studied compounds are adsorbed onto TiO_2.[17] Interestingly, *cis*-Zn2U2A/TiO_2 showed a blue- and red-shifted split Soret band compared to its monomer in THF, thus indicating a mixture of H- and J-type aggregation.[17b,18]

Electrochemical Properties and Energy Levels

Cyclic voltammetry (CV) measurements in degassed THF with 0.1 M $TBAPF_6$ as an electrolyte showed well-resolved and reversible first oxidation potentials for all of the studied zinc porphyrins; selected CVs are shown in Figure 2. The oxidation potentials (Table 1) indicate that the peripheral substituents at the *meso* positions have a significant impact on the redox potential. A lowest first oxidation potential of 0.69 V has been observed for *cis*-Zn2U2A, whereas *cis*-Zn2TPA2A shows two successive oxidation steps at 0.70 and 0.88 V, which corresponded to the one-electron oxidation of the triphenylamino group and the one-electron oxidation of the porphyrin core, respectively.[10c] The oxidation potentials

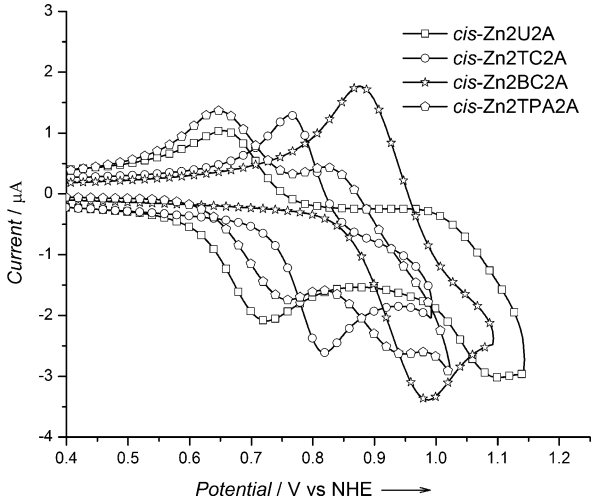

Figure 2. CVs of *cis*-Zn2U2A, *cis*-Zn2TC2A, *cis*-Zn2BC2A, and *cis*-Zn2TPA2A.

of all of the studied porphyrin dyes were more positive than that of the I^-/I_3^- redox couple, thus assuring effective reductive regeneration of the oxidized porphyrin dyes in DSSC devices. The excited-state oxidation potentials (E_{ox}*) were obtained from the relationship $E_{ox}^* = E_{ox1} - E_{0\text{-}0}$, where E_{ox1} is the first oxidation potential of a porphyrin dye and $E_{0\text{-}0}$ is the zero–zero excitation energy, as obtained from the intersection of the absorption and emission bands. The calculated E_{ox}* energy levels of these porphyrins (Table 1) are more negative than the conduction band (CB) of TiO_2, thus providing the necessary driving force for electron injection from the excited state of the dye into the CB of TiO_2. The systematic energy-level diagram of the studied porphyrins versus the TiO_2 conduction band and the I^-/I_3^- redox potential is shown in Figure 3, thus demonstrating the feasibility of electron injection into the conduction band of TiO_2 and dye regeneration by the electrolyte.[19] Although the factors that determine the overall power-conversion efficiency are complicated, the larger potential difference of 0.53 V between E_{ox} and the I^-/I_3^- redox potential for *cis*-Zn2BC2A

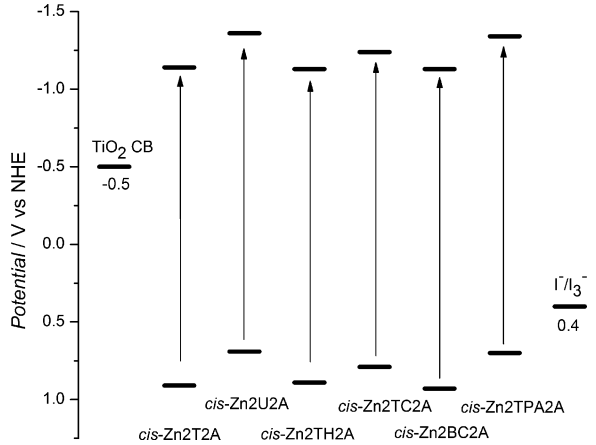

Figure 3. Energy-level diagram of the 2D-π-2A porphyrin dyes.

than, for example, 0.29 V for *cis*-Zn2U2A, should result in thermodynamically more favorable dye regeneration and has a positive impact on their photon-to-energy-conversion efficiencies. The fact that *cis*-Zn2BC2A showed a higher efficiency (4.07%) than that of *cis*-Zn2U2A (2.85%) is consistent with the influence of this driving force on the conversion efficiency (see below).

Density Functional Theory Calculations

Density functional theory (DFT) calculations of the studied porphyrins were performed at the B3LYP/6-31G level of theory to gain insight into the electronic structures of the frontier orbitals of the porphyrins. Figure 4 shows the electron-density distributions of the studied porphyrins in their respective HOMO−1, HOMO, LUMO, and LUMO+1 molecular orbitals. The studied 2D-π-2A dyes show different electron-density distributions for porphyrins with or without electron-donating amino moieties. The electron density on the HOMO and HOMO−1 orbitals predominantly resides on the electron-donating TPA or carbazole groups in *cis*-Zn2TC2A, *cis*-Zn2BC2A, and *cis*-Zn2TPA2A, whereas it predominantly resides on the porphyrin core in *cis*-Zn2T2A, *cis*-Zn2U2A, and *cis*-Zn2TH2A. This result implies an improved charge separation and a better charge-injection efficiency for the dual push-and-pull *cis*-Zn2TC2A, *cis*-Zn2BC2A, and *cis*-Zn2TPA2A dyes upon photoexcitation.

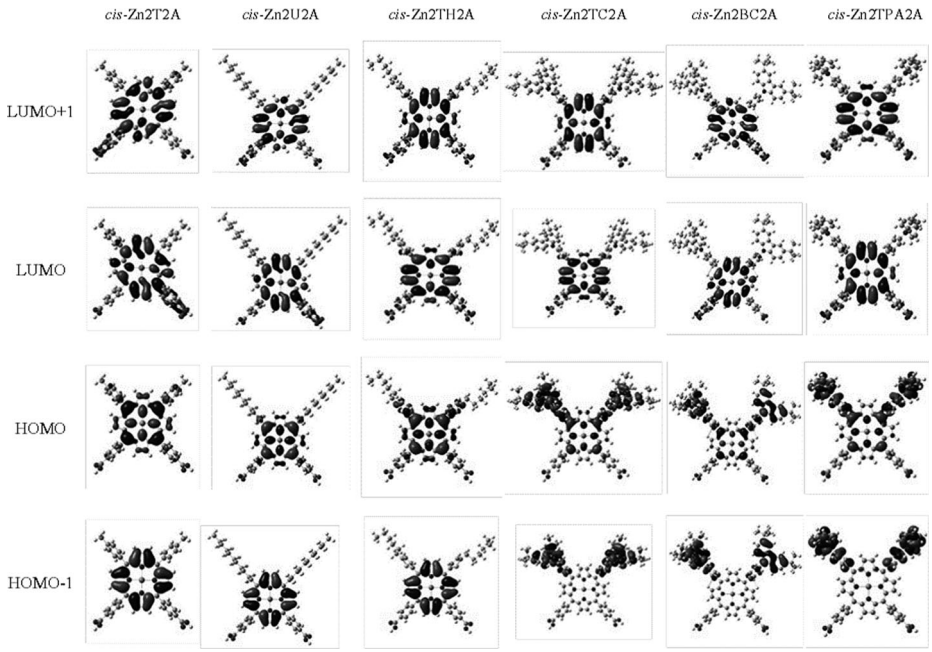

Figure 4. Molecular orbital diagrams of the studied porphyrins as obtained from DFT calculations.

ATR-FTIR Spectroscopy

ATR-FTIR spectroscopy has been utilized as one of the most important tools for probing the number and mode of carboxylate groups that are anchored onto TiO_2.[20] Herein, the ATR-FTIR spectra of neat zinc-porphyrin samples were contrasted with spectra of zinc porphyrins that were adsorbed onto TiO_2. Comparative spectra of representative samples are shown in Figure 5. The spectra of neat *cis*-Zn2U2A and *cis*-Zn2TPA2A show strong ν(C=O) stretches at 1686 and 1690 cm^{-1}, respectively, whereas $\nu_{sym}(COO^-)$ and $\nu_{asym}(COO^-)$ stretches are expected to be observed at about 1400 and 1600 cm^{-1}, respectively. In the comparative spectra of *cis*-Zn2U2A/TiO_2 and *cis*-Zn2TPA2A/TiO_2, the ν-(C=O) stretches completely disappear, accompanied by a noticeable increasing in the stretching peaks of $\nu_{sym}(COO^-)$ and $\nu_{asym}(COO^-)$ at about 1400 and 1600 cm^{-1}, respectively. The observations noted above indicate that both *p*-carboxyphenyl groups at the *meso* positions of the zinc porphyrins are used for bonding onto TiO_2. The same observations are found in the remaining porphyrins, that is, *cis*-Zn2T2A, *cis*-Zn2TH2A, *cis*-Zn2TC2A, and *cis*-Zn2BC2A (see the Supporting Information, Figure S1). Based on these above analyses, the proposed dual-anchoring mode for the attachment of the porphyrins onto TiO_2 is shown in Figure 5c. The observed ATR-FTIR data and the proposed mode of attachment of the studied porphyrins are consistent with literature reports.[21]

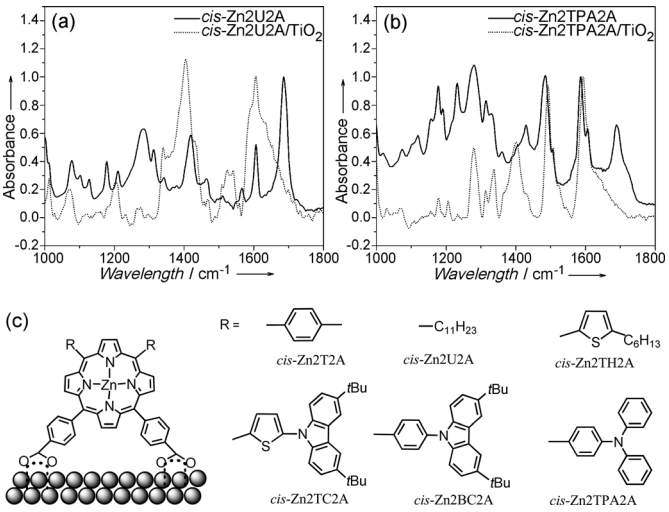

Figure 5. ATR-FTIR spectra of a) *cis*-Zn2U2A and *cis*-Zn2U2A/TiO_2 and b) *cis*-Zn2TPA2A and *cis*-ZnTPA2A/TiO_2; the ATR-FTIR spectra of the porphyrins on TiO_2 are normalized for comparison. c) Possible modes of attachment of 2D-π-2A porphyrins onto TiO_2. For demonstration purpose only, the relative sizes of the molecules and nanoparticles are not correlated in real dimensions.

X-ray Photoelectron Spectroscopy (XPS)

To gain more insight into the adsorption mode of the porphyrins on TiO_2, XPS was performed for *cis*-Zn2BC2A/TiO_2. The O 1s photoelectron spectrum (Figure 6) exhibits two distinct oxygen peaks at 530.3 and 532.4 eV. The oxygen atom on the TiO_2 surface gives the most intense peak at

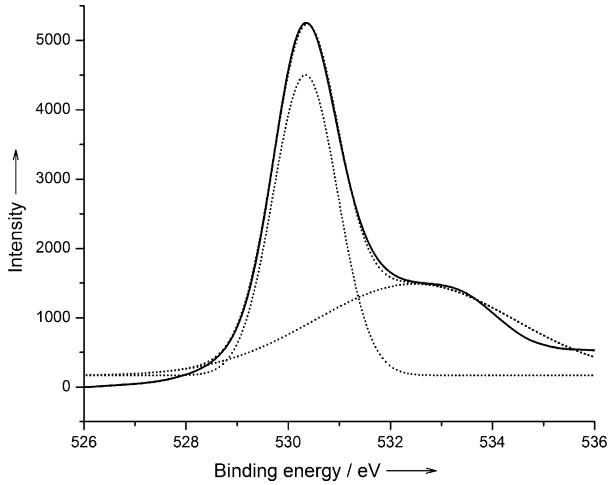

Figure 6. XPS O 1s spectrum of *cis*-Zn2BC2A/TiO_2.

530.3 eV and the minor peak at 532.4 eV originates from the oxygen atoms of carboxylate groups that are attached onto the TiO_2 surface through a bidentate mode of attachment. The spectroscopic pattern and binding energies are in agreement with literature data on dual-*p*-carboxyphenyl-anchored porphyrin dyes.[13a,22]

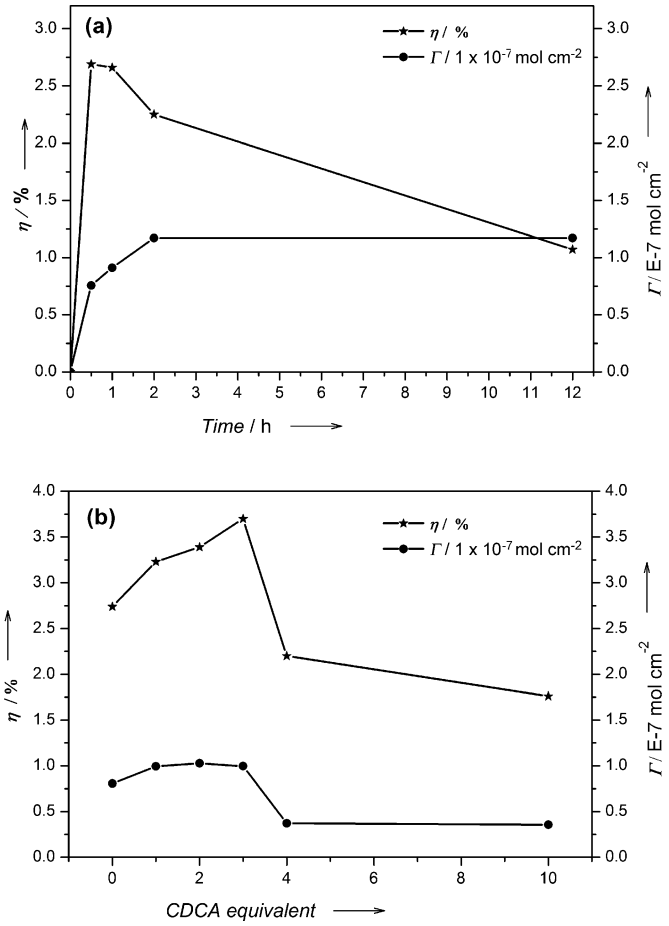

Figure 7. a) Time-dependent plots of efficiency and dye surface density (Γ) of *cis*-Zn2TPA2A. b) Dependence of efficiency and dye surface density (Γ) of *cis*-Zn2TPA2A on the number of equivalents of CDCA.

Photovoltaic Measurements

We optimized the cell performance by examining the immersion time and the chenodeoxycholic acid (CDCA) ratio for *cis*-Zn2TPA2A as a representative example. Firstly, without adding CDCA, the photovoltaic performance of *cis*-Zn2TPA2A was checked after immersion times of 0.5, 1, 2, and 12 h. Figure 7a shows time-dependent plots of the efficiency and dye surface density (Γ) of *cis*-Zn2TPA2A. The increase in immersion time after 0.5 h leads to an increase in the dye surface density up to a highest value after about 2 h. A highest efficiency of 2.69 % was observed at 0.5 h and then decreased progressively up to 12 h. The decrease in efficiency after 0.5 h might be the consequence of dye aggregation upon extended immersion time.[23]

The performance of *cis*-Zn2TPA2A was further improved by adding CDCA as a co-adsorbent to decrease the aggregation. The cell performance of *cis*-Zn2TPA2A was checked by adding 0, 1, 2, 3, 4, and 10 equivalents of CDCA to the immersion solution. The addition of CDCA effectively improved the power-conversion efficiency of *cis*-Zn2TPA2A by obstructing the dye aggregation. Figure 7b shows that the efficiency and dye loading vary with the addition of CDCA. The addition of up to three equivalents of CDCA decreased the dye aggregation and improved the efficiency. Interestingly, against conventional wisdom, the addition of less than three equivalents of CDCA did not decrease the dye density in this case. However, the presence of more than three equivalents of CDCA sharply decreased the dye loading and, hence, caused a drop in efficiency. We assume that, because of a similar binding mode and comparable molecular occupancy volumes, similar trends in immersion time and CDCA concentration with power-conversion efficiency are expected for these zinc-porphyrin dyes.

From these above two experiments, optimized conditions, that is, the addition of three molar equivalents of CDCA with an immersion time of 0.5 h, are obtained. The photovoltaic performance of all of the studied porphyrins under optimized conditions are summarized in Table 2. The *I–V* curves of all of the porphyrins are shown in Figure 8. Depending on the electronic structure of the *meso* substituents, the η values vary within the range 2.42–4.07 %, with J_{SC} and V_{OC} values within the ranges 6.87–9.81 mA cm^{-2} and 0.57–0.63 V, respectively. Highest efficiencies of 4.07 % and 3.64 % were obtained by using *cis*-Zn2BC2A and *cis*-

Table 2. Photovoltaic properties of the 2D-π-2A porphyrins.

Dye	J_{SC} [mA cm^{-2}]	V_{OC} [V]	*FF* [%]	η [%]	Γ [nmol cm^{-2}]
cis-Zn2T2A	7.52	0.57	65	2.78	90
cis-Zn2U2A	8.50	0.58	58	2.85	77
cis-Zn2TH2A	7.92	0.58	69	3.18	69
cis-Zn2TC2A	6.87	0.58	68	2.72	87
cis-Zn2BC2A	9.81	0.63	66	4.07	71
cis-Zn2TPA2A	9.18	0.59	67	3.64	82

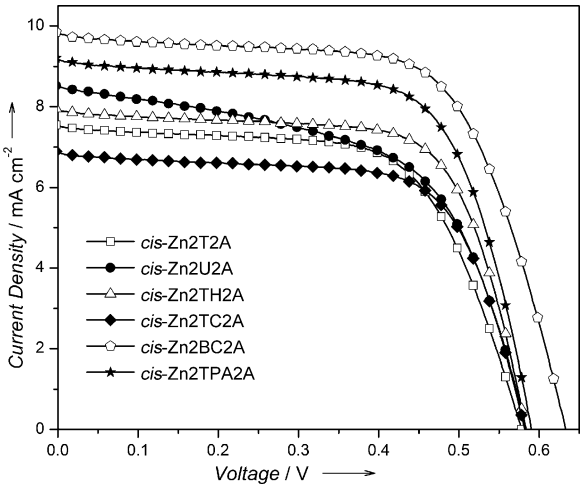

Figure 8. *I–V* curves of studied porphyrin-sensitized solar cells under one-sun illumination.

Zn2TPA2A as the sensitizers, respectively. Presumably, the presence of strongly electron-donating carbazole and triphenylamine moieties facilitate the electron injection. However, without a conclusive dye-adhesion image, the possibility of having tilted porphyrin molecules to shorten the distance between the porphyrin core and the semiconductor layer, thus allowing fast electron injection, cannot be ruled out.[24] Some noticeable observations among the studied dyes are: 1) the linking of the electron-donating carbazole to the porphyrin core through a *para*-phenylene group results in a higher efficiency than the linking through the α-carbon atoms of a thiophene group; 2) the hexyl chain that is attached onto the α-carbon atom of the *meso*-thiophene substituent decreases the aggregation and improves the overall conversion efficiency; and 3) the efficiency of a device that is sensitized by the porphyrin with undecyl groups at the *meso* positions is comparable to that with tolyl *meso* substituents. As shown in Figure 9, the trends in incident-photon-to-current efficiency (IPCE) values and *I–V* curves are roughly consistent. The lower-performing *cis*-Zn2T2A shows lower IPCE percentages, whereas the highly efficient *cis*-Zn2BC2A and *cis*-Zn2TPA2A show the highest IPCEs. This result implies that *cis*-Zn2T2A has lower electron-collection and electron-injection efficiencies compared to *cis*-Zn2BC2A and *cis*-Zn2TPA2A, which directly reflects the overall efficiencies.[25]

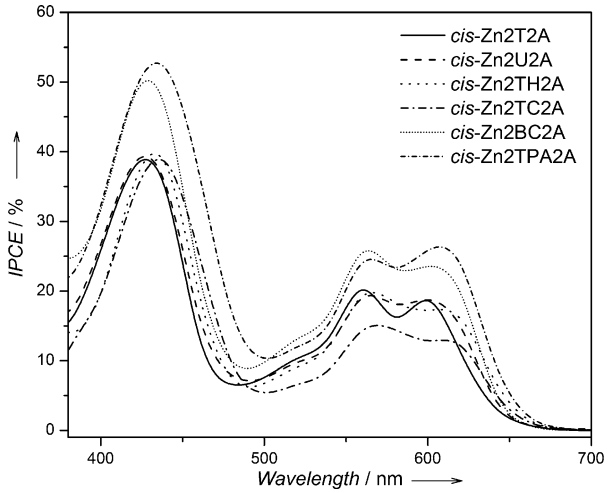

Figure 9. IPCE curves of studied 2D-π-2A porphyrin sensitizers.

The porphyrins on TiO_2 films were desorbed by using a 0.2 M aqueous solution of KOH in THF and the absorbance was measured to determine the dye-loading density. The trends in the dye-loading densities of the porphyrins listed in Table 2 are not of the same order as the trends in efficiency. Despite their low dye densities, *cis*-2BC2A and *cis*-2TPA2A gave better performances, with higher J_{SC} and V_{OC} values. Notably, more than 24 h exposure to commonly used 0.1 M aqueous solution of KOH in THF (2:8, v/v) was unable to completely desorb the dyes from TiO_2 for this series of zinc-porphyrin dyes. Instead, a 0.2 M aqueous solution of KOH in THF (2:8, v/v) was used to desorb the dye from TiO_2. The requirement of a higher concentration of the base to desorb the dye from TiO_2 provides further evidence of a stronger adhesion of the dual-arm-anchoring porphyrin dyes than the porphyrin dyes that possessed a single anchoring group.

Stability Study

With high efficiency, long-term stability is the most-important factor for the commercialization of DSSC. The photostability of these dyes was examined by using the easiest literature procedure.[26] The TiO_2 photoanode films of Zn3TPA1A (for the structure and synthesis of Zn3TPA1A, see the Supporting Information), *cis*-Zn2TPA2A, and *cis*-Zn2BCA2A, after irradiation under standard one-sun illumination, were checked by recording the absorption spectra after specific time intervals. Figure 10 shows absorption curves of Zn3TPA1A, *cis*-Zn2TPA2A, and *cis*-Zn2BC2A after irradiation for 0, 5, and 30 min. The absorbance of the dyes decreased by various amounts, depending on the *meso* substituents. The decrease in the absorbance was more dramatic for Zn3TPA1A than for *cis*-Zn2TPA2A and *cis*-Zn2BC2A, thus suggesting that the *cis*-Zn2TPA2A and *cis*-Zn2BC2A dyes, which possessed a 2D-π-2A framework, are more stable than Zn3TPA1A.

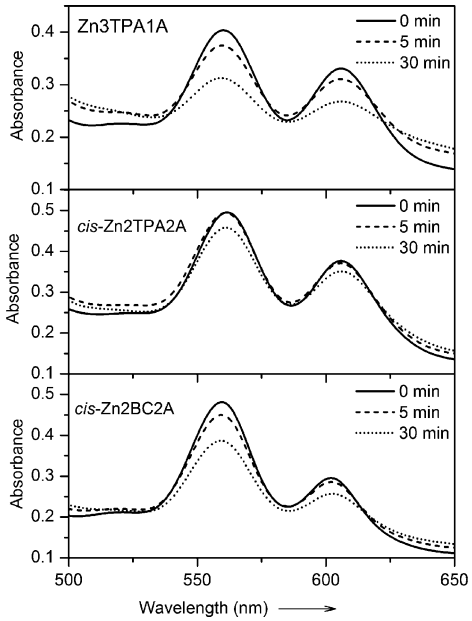

Figure 10. Absorption spectra of Zn3TPA1A, *cis*-Zn2TPA2A, and *cis*-Zn2BC2A that were adsorbed onto TiO_2 films after irradiation for 0, 5, and 30 min.

Conclusions

New dual donor–acceptor (2D-π-2A) porphyrin sensitizers have been synthesized from readily available starting materials in good yields. The synthesis of these sensitizers, which involved one-pot, two-step condensation reactions, followed by high-yielding metalation and hydrolysis steps, employed the minimum possible steps for the preparation of carboxyphenyl-zinc-porphyrin complexes. Most of the zinc porphyrins in this work adsorbed onto a TiO_2 film with J-type aggregation and caused a red-shift, except for *cis*-Zn2U2A, which showed a mixture of H- and J-type aggregation. The electrochemical properties and energy-level diagrams of these porphyrins show that they are effective sensitizing dyes for application in DSSCs. ATR-FTIR spectroscopy of 2D-π-2A framework porphyrins that were adsorbed onto TiO_2 confirmed dye chelation to the TiO_2 surface with a double-arm-binding mode, which ensures efficient electron transfer and strong attachment. A highest efficiency of 4.07% has been observed for the DSSC, by using *cis*-Zn2BC2A as the sensitizer, owing to its higher molecular extinction coefficient, IPCE, short-circuit potential, and open-circuit voltage. The stability study as examined from the absorption spectra demonstrates better photostability of the dual-arm-anchored Zn2TPA2A compared to their mono-anchored analogues.

Experimental Section

Syntheses

The zinc porphyrins were synthesized in three steps, that is, mixed condensation, zinc metalation, and hydrolysis, according to literature procedures. For detailed synthetic procedures and characterization data, see the Supporting Information. All of the porphyrins were characterized by optical spectroscopy, ATR-FTIR, NMR spectroscopy, and HRMS. All of the chemicals were purchased from Acros Organics or Sigma Aldrich and used without further purification. ^{1}H NMR spectra were recorded on a Bruker 400 MHz spectrometer in $CDCl_3$ ($\delta = 7.26$ ppm), [D_6]DMSO ($\delta = 2.50$ ppm), or CD_3OD ($\delta = 3.31$ ppm); ^{13}C NMR spectra were recorded in [D_6]DMSO ($\delta = 40.0$ ppm) or CD_3OD ($\delta = 49.0$ ppm). Chemical shifts are reported in ppm. Coupling constants (J) are reported in Hz. The signals are described as s = singlet, d = doublet or dd = doublet of doublet. HRMS (FAB or ESI) was performed on a JMS-700 double-focusing mass spectrometer (JEOL, Tokyo, Japan). Flash chromatography was performed on silica gel (40–63 μm, Merck). Analytical TLC was performed on silica-gel plates (Merck). Melting points were recorded on a capillary melting-point apparatus (Electrothermal).

Optical Spectroscopy

UV/Vis absorption spectra of the porphyrins in THF and adsorbed onto TiO_2 electrodes were recorded on a JASCO V-670 UV/Vis/NIR spectrophotometer. For the absorption spectra of the thin films on TiO_2, TiO_2 films (area: 1×1 cm^2) were prepared with thicknesses of about 1 μm to obtain comparable shapes and peak positions. The films were immersed in 2×10^{-4} M solutions of the porphyrins in THF for 12 h and the films were rinsed with THF, dried, and the absorbance was measured. Steady-state fluorescence spectra were acquired on a Varian Cary Eclipse fluorescence spectrophotometer.

Cyclic Voltammetry

The CV measurements of all of the porphyrins were performed on a CHI 600D electrochemical analyzer (CH Instruments, Austin, TX, USA) in degassed THF with 0.1 M $TBAPF_6$ as a supporting electrolyte. The cell assembly consisted of a glassy carbon working electrode, Ag wire as a reference electrode, and platinum wire as the auxiliary electrode. A ferrocene/ferrocenium redox couple was used as an internal reference.

DFT Calculations

Geometry optimizations and the electronic structures of the porphyrins were performed by using DFT at the B3LYP level of theory with the 6-31G basis set in the Gaussian 09 program package.

ATR-FTIR Measurements

ATR-FTIR spectra of the zinc porphyrins were recorded on a VERTEX 70 spectrometer with a Golden Gate diamond ATR accessory on solid powders of the porphyrin samples. For the preparation of the samples with zinc porphyrins adsorbed onto TiO_2, a 5×10^{-4} M solution of the porphyrin in THF was mixed with TiO_2 powder (5 mg) and left to stand for 12 h. Afterwards, the excess solvent was dripped out by pipet. TiO_2 powder was washed twice with THF and dried in vacuo and the obtained powder sample was used for the measurements. ATR-FTIR spectra of the zinc porphyrin that was adsorbed onto TiO_2 were recorded at a resolution of 4 cm^{-1} and averaged over 320 scans.

XPS Measurements

XPS data were recorded on an Omicron ESCA spectrometer with a dual-anode $Al_{K\alpha}$ X-ray source. The spectrum was calibrated to the C 1s spectrum at 285 eV. The signals were deconvoluted by using the Gaussian functions with the OriginPro 8.1 program. For the preparation of a sample, TiO_2 films (area: 1×1 cm^2, thickness: 3–4 μm) were immersed in a 2×10^{-4} M solution of *cis*-Zn2BC2A in THF for 0.5 h, rinsed with THF, and heated at 120 °C before use.

Photovoltaic Measurements

TiO_2 photoanode films were purchased from Yingkou Opvtech New Energy Co. Ltd. Liaoning, China. The films, which were prepared by using the screen-printing method, were composed of a transparent layer (thickness≈12 μm), a scattering layer (thickness≈4 μm), and a working area of 0.4×0.4 cm^2 and were used directly upon receipt. The films were pretreated according to the following activation procedures before use: Heating at 100 °C for 22 min, at 110 °C for 60 min, at 450 °C for 68 min, at 500 °C 60 min, at 250 °C for 60 min, cooling at 80 °C and keeping at 80 °C before immersion. The TiO_2 films were immersed in a 2×10^{-4} M solution of the porphyrin in THF and a 6×10^{-4} M solution of CDCA at 50 °C. The dye-sensitized TiO_2 films were washed with THF, dried in hot air, and used as the working electrode. The counter electrode was prepared on an indium-doped tin-oxide (ITO, 5.5 Ω/□) glass substrate (typical size: 1.0×1.5 cm^2) by spin-coating a H_2PtCl_6/isopropanol solution through thermal decomposition at 380 °C for 0.5 h. To fabricate the DSSC device, the two electrodes were tightly clipped together into a sandwich-type cell that was spaced by a 40 μm film spacer. A thin layer of electrolyte, which contained 0.05 M I_2, 0.1 M lithium iodide (LiI), 0.6 M dimethyl-propyl-benzimidiazole iodide (DMPII), and 0.6 M 4-tert-butylpyridine (TBP) in dry CH_3CN, was introduced into the space between the two electrodes. The photo-electrochemical characterizations on the solar cells were performed on an Oriel Class A solar simulator (Oriel 91195A, Newport Corp.). Photocurrent–voltage characteristics of the DSSCs were recorded on a potentiostat/galvanostat (CHI650B, CH Instruments, Inc.) at a light intensity of 100 mW cm^{-2} and calibrated to an Oriel reference solar cell (Oriel 91150, Newport Corp.). The monochromatic quantum efficiency was recorded on a monochromator (Oriel 74100, Newport Corp.) under short-circuit conditions. The intensity of each wavelength was within the range 1–3 mW cm^{-2}.

Stability Study

For the stability study, TiO_2 thin films with areas of 1×1 cm^2 and thicknesses of 3–4 μm were used. The films were immersed in a 2×10^{-4} M solution of the porphyrin in THF for 0.5 h, dried, and the absorbance was measured. Then, the same films were irradiated under standard one-sun illumination for 5 min and 30 min and the absorbance was measured again.

Acknowledgements

The authors greatly acknowledge financial support from the National Science Council (Taiwan) and the Academia Sinica. Mass spectroscopy analysis was performed by the Mass Spectrometry Facility of the Institute of Chemistry, Academia Sinica (Taiwan). Help from Dr. Jiann-T'suen Lin with the measurements and instrumentation is greatly appreciated.

[1] B. O'Regan, M. Gratzel, *Nature* **1991**, *353*, 737–740.
[2] a) A. Hagfeldt, G. Boschloo, L. Sun, L. Kloo, H. Pettersson, *Chem. Rev.* **2010**, *110*, 6595–6663; b) L.-L. Li, E. W.-G. Diau, *Chem. Soc. Rev.* **2013**, *42*, 291–304; c) W. M. Campbell, A. K. Burrell, D. L. Officer, K. W. Jolley, *Coord. Chem. Rev.* **2004**, *248*, 1363–1379; d) A. Mishra, M. K. R. Fischer, P. Bäuerle, *Angew. Chem.* **2009**, *121*, 2510–2536; *Angew. Chem. Int. Ed.* **2009**, *48*, 2474–2499; e) H. Imahori, T. Umeyama, S. Ito, *Acc. Chem. Res.* **2009**, *42*, 1809–1818; f) Y. Ooyama, Y. Harima, *Eur. J. Org. Chem.* **2009**, 2903–2934.
[3] M. K. Nazeeruddin, F. De Angelis, S. Fantacci, A. Selloni, G. Viscardi, P. Liska, S. Ito, B. Takeru, M. Grätzel, *J. Am. Chem. Soc.* **2005**, *127*, 16835–16847.
[4] F. Gao, Y. Wang, D. Shi, J. Zhang, M. Wang, X. Jing, R. Humphry-Baker, P. Wang, S. M. Zakeeruddin, M. Grätzel, *J. Am. Chem. Soc.* **2008**, *130*, 10720–10728.
[5] Q. Yu, Y. Wang, Z. Yi, N. Zu, J. Zhang, M. Zhang, P. Wang, *ACS Nano* **2010**, *4*, 6032–6038.
[6] L. Han, A. Islam, H. Chen, C. Malapaka, B. Chiranjeevi, S. Zhang, X. Yang, M. Yanagida, *Energy Environ. Sci.* **2012**, *5*, 6057–6060.
[7] S. Ito, H. Miura, S. Uchida, M. Takata, K. Sumioka, P. Liska, P. Comte, P. Pechy, M. Gratzel, *Chem. Commun.* **2008**, 5194–5196.
[8] W. Zeng, Y. Cao, Y. Bai, Y. Wang, Y. Shi, M. Zhang, F. Wang, C. Pan, P. Wang, *Chem. Mater.* **2010**, *22*, 1915–1925.
[9] W. M. Campbell, K. W. Jolley, P. Wagner, K. Wagner, P. J. Walsh, K. C. Gordon, L. Schmidt-Mende, M. K. Nazeeruddin, Q. Wang, M. Grätzel, D. L. Officer, *J. Phys. Chem. C* **2007**, *111*, 11760–11762.
[10] a) S.-L. Wu, H.-P. Lu, H.-T. Yu, S.-H. Chuang, C.-L. Chiu, C.-W. Lee, E. W.-G. Diau, C.-Y. Yeh, *Energy Environ. Sci.* **2010**, *3*, 949–955; b) C.-W. Lee, H.-P. Lu, C.-M. Lan, Y.-L. Huang, Y.-R. Liang, W.-N. Yen, Y.-C. Liu, Y.-S. Lin, E. W.-G. Diau, C.-Y. Yeh, *Chem. Eur. J.* **2009**, *15*, 1403–1412; c) C.-P. Hsieh, H.-P. Lu, C.-L. Chiu, C.-W. Lee, S.-H. Chuang, C.-L. Mai, W.-N. Yen, S.-J. Hsu, E. W.-G. Diau, C.-Y. Yeh, *J. Mater. Chem.* **2010**, *20*, 1127–1134; d) K. K. Pasunooti, J.-L. Song, H. Chai, P. Amaladass, W.-Q. Deng, X.-W. Liu, *J. Photochem. Photobiol. A* **2011**, *218*, 219–225; e) T. Bessho, S. M. Zakeeruddin, C.-Y. Yeh, E. W.-G. Diau, M. Grätzel, *Angew. Chem.* **2010**, *122*, 6796–6799; *Angew. Chem. Int. Ed.* **2010**, *49*, 6646–6649; f) H.-P. Lu, C.-L. Mai, C.-Y. Tsia, S.-J. Hsu, C.-P. Hsieh, C.-L. Chiu, C.-Y. Yeh, E. W.-G. Diau, *Phys. Chem. Chem. Phys.* **2009**, *11*, 10270–10274.
[11] A. Yella, H.-W. Lee, H. N. Tsao, C. Yi, A. K. Chandiran, M. K. Nazeeruddin, E. W.-G. Diau, C.-Y. Yeh, S. M. Zakeeruddin, M. Grätzel, *Science* **2011**, *334*, 629–634.
[12] R. Ambre, K.-B. Chen, C.-F. Yao, L. Luo, E. W.-G. Diau, C.-H. Hung, *J. Phys. Chem. C* **2012**, *116*, 11907–11916.
[13] a) H. Imahori, Y. Matsubara, H. Iijima, T. Umeyama, Y. Matano, S. Ito, M. Niemi, N. V. Tkachenko, H. Lemmetyinen, *J. Phys. Chem. C* **2010**, *114*, 10656–10665; b) J. N. Clifford, G. Yahioglu, L. R. Milgrom, J. R. Durrant, *Chem. Commun.* **2002**, *0*, 1260–1261.
[14] T. S. Balaban, A. Eichhöfer, J.-M. Lehn, *Eur. J. Org. Chem.* **2000**, 4047–4057.
[15] M. Kozaki, A. Uetomo, S. Suzuki, K. Okada, *Org. Lett.* **2008**, *10*, 4477–4480.
[16] C. Luo, D. M. Guldi, H. Imahori, K. Tamaki, Y. Sakata, *J. Am. Chem. Soc.* **2000**, *122*, 6535–6551.
[17] a) C.-F. Lo, L. Luo, E. W.-G. Diau, I. J. Chang, C.-Y. Lin, *Chem. Commun.* **2006**, *0*, 1430–1432; b) C. Y. Lee, C. She, N. C. Jeong, J. T. Hupp, *Chem. Commun.* **2010**, *46*, 6090–6092.
[18] C.-M. Lan, H.-P. Wu, T.-Y. Pan, C.-W. Chang, W.-S. Chao, C.-T. Chen, C.-L. Wang, C.-Y. Lin, E. W.-G. Diau, *Energy Environ. Sci.* **2012**, *5*, 6460–6464.
[19] a) M. K. Panda, G. D. Sharma, K. R. Justin Thomas, A. G. Coutsolelos, *J. Mater. Chem.* **2012**, *22*, 8092–8102; b) C.-L. Wang, C.-M. Lan, S.-H. Hong, Y.-F. Wang, T.-Y. Pan, C.-W. Chang, H.-H. Kuo, M.-Y. Kuo, E. W.-G. Diau, C.-Y. Lin, *Energy Environ. Sci.* **2012**, *5*, 6933–6940.
[20] a) M. K. Nazeeruddin, R. Humphry-Baker, D. L. Officer, W. M. Campbell, A. K. Burrell, M. Grätzel, *Langmuir* **2004**, *20*, 6514–6517; b) P.-A. Bouit, M. Marszalek, R. Humphry-Baker, R. Viruela, E. Ortí, S. M. Zakeeruddin, M. Grätzel, J. L. Delgado, N. Martín, *Chem. Eur. J.* **2012**, *18*, 11621–11629; c) A. Abbotto, N. Manfredi, C. Marinzi, F. De Angelis, E. Mosconi, J.-H. Yum, Z. Xianxi, M. K. Nazeeruddin, M. Gratzel, *Energy Environ. Sci.* **2009**, *2*, 1094–1101; d) N. Lu, J.-S. Shing, W.-H. Tu, Y.-C. Hsu, J. T. Lin, *Inorg. Chem.* **2011**, *50*, 4289–4294; e) D. Heredia, J. Natera, M. Gervaldo, L. Otero, F. Fungo, C.-Y. Lin, K.-T. Wong, *Org. Lett.* **2010**, *12*, 12–15.
[21] J. Rochford, D. Chu, A. Hagfeldt, E. Galoppini, *J. Am. Chem. Soc.* **2007**, *129*, 4655–4665.
[22] a) S. Eu, S. Hayashi, T. Umeyama, Y. Matano, Y. Araki, H. Imahori, *J. Phys. Chem. C* **2008**, *112*, 4396–4405; b) A. Kira, Y. Matsubara, H. Iijima, T. Umeyama, Y. Matano, S. Ito, M. Niemi, N. V. Tkachenko, H. Lemmetyinen, H. Imahori, *J. Phys. Chem. C* **2010**, *114*, 11293–11304.
[23] a) S. Eu, S. Hayashi, T. Umeyama, A. Oguro, M. Kawasaki, N. Kadota, Y. Matano, H. Imahori, *J. Phys. Chem. C* **2007**, *111*, 3528–

3537; b) H. Imahori, S. Hayashi, H. Hayashi, A. Oguro, S. Eu, T. Umeyama, Y. Matano, *J. Phys. Chem. C* **2009**, *113*, 18406 – 18413.
[24] a) H. Imahori, S. Kang, H. Hayashi, M. Haruta, H. Kurata, S. Isoda, S. E. Canton, Y. Infahsaeng, A. Kathiravan, T. r. Pascher, P. Chábera, A. P. Yartsev, V. Sundström, *J. Phys. Chem. A* **2011**, *115*, 3679 – 3690; b) H. Imahori, T. Umeyama, K. Kurotobi, Y. Takano, *Chem. Commun.* **2012**, *48*, 4032 – 4045.
[25] a) V. Aranyos, H. Grennberg, S. Tingry, S.-E. Lindquist, A. Hagfeldt, *Sol. Energy Mater. Sol. Cells* **2000**, *64*, 97 – 114; b) K. Hara, H. Sugihara, Y. Tachibana, A. Islam, M. Yanagida, K. Sayama, H. Arakawa, G. Fujihashi, T. Horiguchi, T. Kinoshita, *Langmuir* **2001**, *17*, 5992 – 5999.
[26] a) R. Katoh, A. Furube, S. Mori, M. Miyashita, K. Sunahara, N. Koumura, K. Hara, *Energy Environ. Sci.* **2009**, *2*, 542 – 546; b) Y. Wu, M. Marszalek, S. M. Zakeeruddin, Q. Zhang, H. Tian, M. Gratzel, W. Zhu, *Energy Environ. Sci.* **2012**, *5*, 8261 – 8272.

Received: March 12, 2013
Revised: April 19, 2013
Published online: July 3, 2013

